Supplementary materials of Biomaterials Science

Yue, Zhao[b,c], Hanming, Yao[b,c], Kege, Yang[b,c], Shiji, Han[b,c], Shangxiang, Chen[b,c], Yaqing, Li[b,c], Shaojie, Chen[b,c], Kaihong, Huang[b,c*], Guoda, Lian[b,c*], Jiajia, Lia,[b,c*].

a. Department of Nephrology, Sun Yat-Sen Memorial Hospital, Sun Yat-Sen University, Guangzhou 510120, Guangdong, China.

E-mail: Lijj9@mail2.sysu.edu.cn

b. Department of Gastroenterology, Sun Yat-sen Memorial Hospital, Sun Yat-sen University, Guangzhou 510120, China.

c. Guangdong Provincial Key Laboratory of Malignant Tumor Epigenetics and Gene Regulation, Sun Yat-sen Memorial Hospital, Sun Yat-sen University, Guangzhou 510120, China.

1. Clinical characteristic of Pancreatic cancer patients.

Human pancreatic cancer samples of 57 patients were obtained from Sun Yat-sen Memorial Hospital. The clinical characteristic was provided as follows. The significant difference could not be found between the high and low α-sma expression groups. Similar results could be found in collagen type I and Fibronectin groups.

Table S1 Clinical characteristic of 57 patients in Sun Yat-sen Memorial Hospital.

Clinical features	α-sma			Collagen Type I			Fibronectin		
	low expression	high expression	*p*	low expression	high expression	*p*	low expression	high expression	*p*
Age(years)			0.483			0.315			0.697
<60	11(19.3%)	16(28.1%)		5(9%)	22(38.6%)		6(10.5%)	21(36.9%)	
≥60	15(26.3%)	15(26.3%)		9(15.6%)	21(36.8%)		8(14.0%)	22(38.60%)	
Gender			0.115			0.544			0.224
Male	12(21.1%)	21(36.8%)		7(12.3%)	26(45.6%)		6(10.5%)	27(47.4%)	
Female	14(24.6%)	10(17.5%)		7(12.3%)	17(29.8%)		8(14.0%)	16(28.1%)	
T status			0.787			0.405			0.929
T2	5(0.09%)	8(14.0%)		5(8.8%)	8(14.0%)		3(5.3%)	10（17.5%）	
T3	13(22.8%)	13(22.8%)		5(8.8%)	21(36.8%)		6（10.5%）	20（35.1%）	
T4	8(14.0%)	10(17.5%)		4(7%)	14(24.6%)		5（8.8%）	13（22.8%）	
LN metastasis			0.5			0.034			0.131
N0	13(22.8%)	13(22.8%)		10(17.5%)	16(28.1%)		9(15.8%)	17(29.8%)	
N1	13(22.8%)	18(31.6%)		4(7%)	27(47.4%)		5(8.8%)	26(45.6%)	
Distant metastasis			0.539			0.478			0.478
M0	21(36.8%)	22(38.6%)		12(21.1%)	31(54.3%)		12(21.1%)	31(54.3%)	
M1	5(8.8%)	9(15.8%)		2(3.5%)	12(21.1%)		2(3.5%)	12(21.1%)	
Clinical stage			0.844			0.124			0.667
I	4(7.0%)	5(8.8%)		5(8.8%)	4(7.0%)		3(5.3%)	6(10.5%)	
II	7(12.3%)	7(12.3%)		3(5.3%)	11(19.2%)		3(5.3%)	11(19.2%)	
III	10(17.5%)	10(17.5%)		4(7.0%)	16(28.1%)		6(10.5%)	14(24.6%)	
IV	5(8.8%)	9(15.8%)		2(3.5%)	12(21.1%)		2(3.5%)	12(21.1%)	

2. The GO analysis of DEGs from RNA sequence

Table S2 GO analysis of differential expression genes from RNA-seq.

ID	Species	GOTERM_BP_DIRECT	GOTERM_CC_DIRECT	GOTERM_MF_DIRECT
LGALS1	Homo sapiens	GO:0007157~heterophilic cell-cell adhesion via plasma membrane cell adhesion molecules,	GO:0005615~extracellular space,	GO:0030246~carbohydrate binding,
C1QTNF4	Homo sapiens		GO:0005615~extracellular space,	GO:0005125~cytokine activity,
WNT2	Homo sapiens	GO:0002053~positive regulation of mesenchymal cell proliferation, GO:0002088~lens development in camera-type eye, GO:0007267~cell-cell signaling, GO:0008284~positive regulation of cell proliferation, GO:0048146~positive regulation of fibroblast proliferation, GO:0060317~cardiac epithelial to mesenchymal transition, GO:0071560~cellular response to transforming growth factor beta stimulus	GO:0005576~extracellular region, GO:0005578~proteinaceous extracellular matrix, GO:0005615~extracellular space, GO:0031012~extracellular matrix	GO:0005109~frizzled binding, GO:0005125~cytokine activity, GO:0005515~protein binding, GO:0048018~receptor agonist activity,
IGLC3	Homo sapiens	GO:0006956~complement activation, GO:0006958~complement activation, classical pathway,	GO:0005576~extracellular region, GO:0005615~extracellular space,	GO:0003823~antigen binding, GO:0004252~serine-type endopeptidase activity, GO:0034987~immunoglobulin receptor binding,
PENK	Homo sapiens	GO:0071560~cellular response to transforming growth factor beta stimulus	GO:0005576~extracellular region,	GO:0001515~opioid peptide activity, GO:0005184~neuropeptide hormone activity, GO:0031628~opioid receptor binding,
TMPRSS6	Homo sapiens	GO:0030198~extracellular matrix organization, GO:0042730~fibrinolysis,	GO:0005615~extracellular space,	GO:0004252~serine-type endopeptidase activity, GO:0005515~protein binding,

3. ATO alleviates the tumor-promoting action of PSCs by decreasing PSCs ECM production.

The statistical histograms of the **Figure 4** were displayed in the **Fig. S1**. While treated with 2.0 μM ATO for 48h, the expression of Collagen Type I, Fibronectin and α-sma in PSCs were the lowest in four groups **(Fig. S1A)**. While co-cultured with PSCs, the wound healing percentage of PANC-1 and MIA PaCa-2 increased, which could be alleviated by 2.0 μM ATO **(Fig. S1B)**.

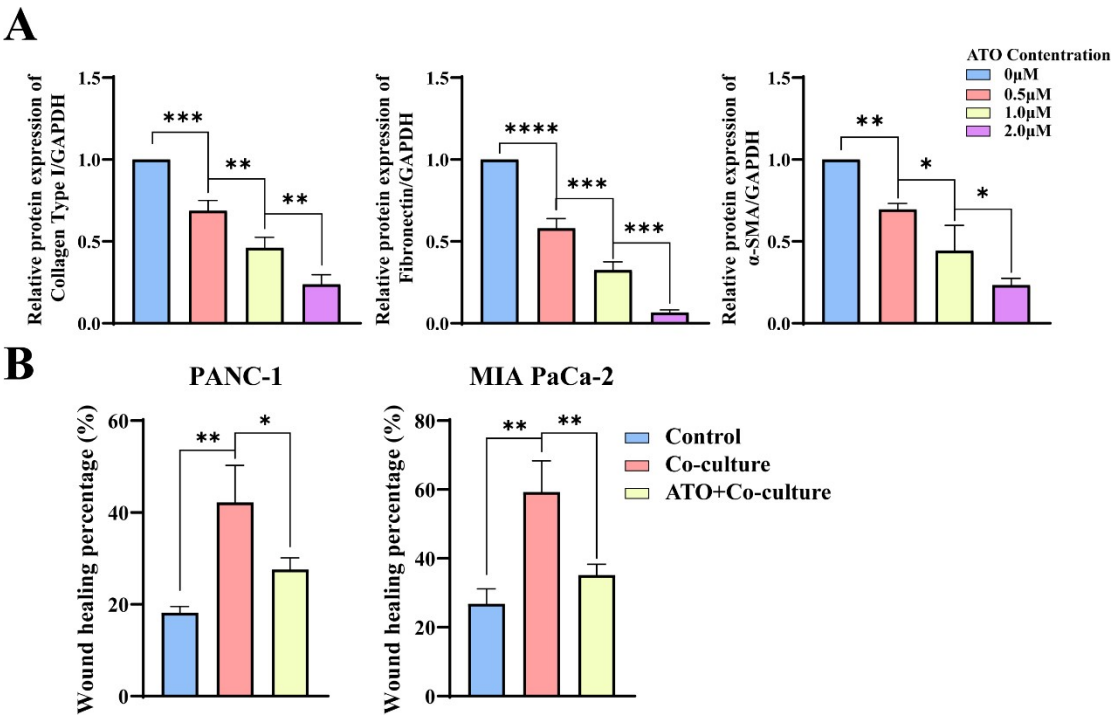

Figure S1. ATO inhibits PSCs activation and alleviates the tumor-promoting function. A. After treated with ATO of different concentration, the proteins expression was detected by Western blot and quantified by Image J. B. The wound healing percentage was utilized to quantify the migration ability of PANC-1 and MIA PaCa-2. All the results were repeated for 3 times. *, $P < 0.05$; **, $P < 0.01$.

4. ATO reverses PSCs activation via PI3K/Akt/AP4/Galecin-1 pathway

While treated with 2.0 μM ATO for 48h, the expression of AP4 and Galectin-1 in PSCs were the lowest in four groups **(Fig. S2A)**. After knock down the expression of Galectin-1 in PSCs, the decrease of Collagen Type I, Fibronectin and α-sma could be found but the expression of AP4 didn't be influenced. However, after transfecting the siRNA of AP4, all the expression of AP4, Galectin-1, Collagen Type I, Fibronectin and α-sma decreased **(Fig. S2B).** Compared with the control group, the expression of PI3K decreased in PSCs treated with LY294002 or ATO, which could be partially alleviated by IGF-1. Similar trends of other proteins expression could be found in different treatments except the AKT expression **(Fig. S2C).**

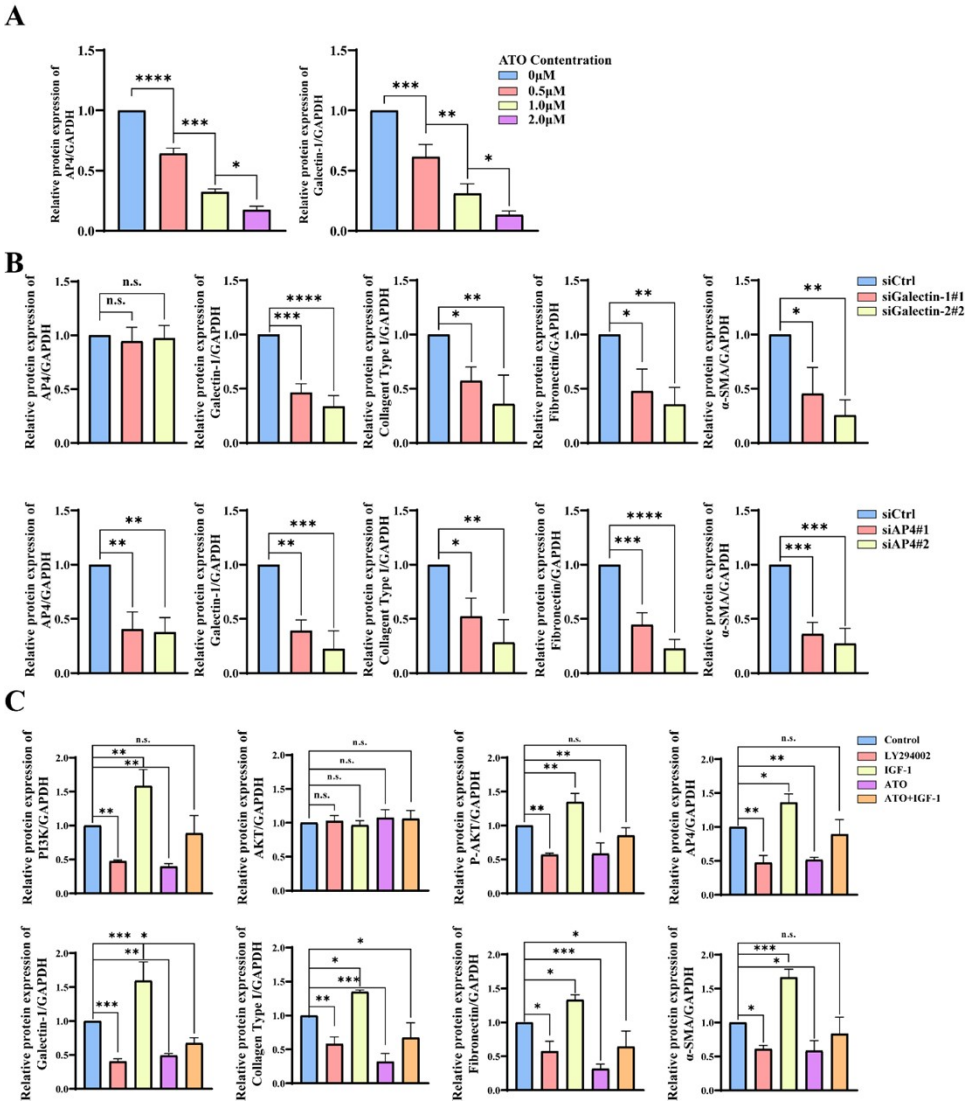

Figure S2. Quantification results of **Figure 5**. All the protein expression in Figure 5 were repeated for 3 times and the Data were represented as MEAN and Standard deviation (SD). *, $P < 0.05$; **, $P < 0.01$; ***, $P < 0.001$; ****, $P < 0.0001$.

5. Supplementary information of scAb-ATO-NPs.

5.1 Materials and equipment.

Arsenic trioxide (purity 99.995%) was purchased from Sigma Chemical Co (USA). 18-Crown-6 (from Sigma-Aldrich) was vacuum-dried overnight at 46 ℃. Ethylene oxide (EO, purity 99%) were obtained from Foshan Kedi Gas Chemical Industry (China). Ethyl acetate was used to purify and obtain DL-lactide (Sigama-Aldrich). All organic solvents were of analytic grade and purchased from Guangzhou Chemical Reagent Factory (China). Varian Unity 300 MHz spectrometer was utilized to record ^{1}H NMR spectra in Chloroform-D1. A Hitachi model H-7650 TEM operated at 80 kV was used to record the transmission electron microscopy (TEM) of nanoparticle.

5.2 Synthesis and characterization of mal-PEG-PDLLA

Synthesis of the maleimide-terminated block copolymer poly (ethylene glycol)-poly (DL-lactide) (mal-PEG-PDLLA) was referenced to the published article.[35] Briefly, the anionic polymerization of oxacyclopropane was performed with an initiator of propylene alcohol and a catalyst of naphthalene potassium to synthesize allyl-PEG-OH, whose molecular weight could reach to 2 kDa. Then in order to get H_2N-PEG-OH, the double bond of allyl-PEG-OH needed to be opened with an initiator of 2-mercaptoethylamine and a catalyst of azodiisobutyronitrile (AIBN). Besides, H_2N-PEG-OH could react with 2-mercaptoethylamine and mal-PEG-OH could be synthesized. Next, a ring-opening polymerization of lactide was performed with an initiator of mal-PEG-OH at 70 ℃, which needed the catalysis of stannous octoate. 24 hours later, the mal-PEG-PDLLA could be synthesized **(Fig. S3A)**.

Mal-PEG-PDLLA were characterized by ^{1}H NMR (Mercury-Plus300) in Chloroform ($CDCl_3$) at 25 °C. The chemical shift of N-methoxycarbonylmaleimide located at 6.7 ppm (a). The chemical shift of PEG (OCH_2CH_2O) and methylidyne (CH) and methyl group (CH_3) of PDLLA appeared at 3.6 ppm (g), 5.2 ppm (h) and 1.6 ppm (i) respectively, which was fit into the expected chemical structure and demonstrated that the block polymer mal-PEG-PDLLA was successfully synthesized **(Fig. S3B)**.

The stability of scAb-ATO-NPs in solution was verified to ensure the application in vivo. Continuous DLS was performed to measure the diameter of the scAb-ATO-NPs during 48hours. In brief, 1ml FBS containing (10%) PBS was added to 24 wells plate. scAb-ATO-NPs was added to PBS and incubated at 37°C. The nanoparticle in 3 wells was collected and measured the mean

diameter every 3 hours. No significant variation of the diameter could be found in for 48 hours, which meant no obvious degradation of the nanoparticle **(Figure S3C)**.

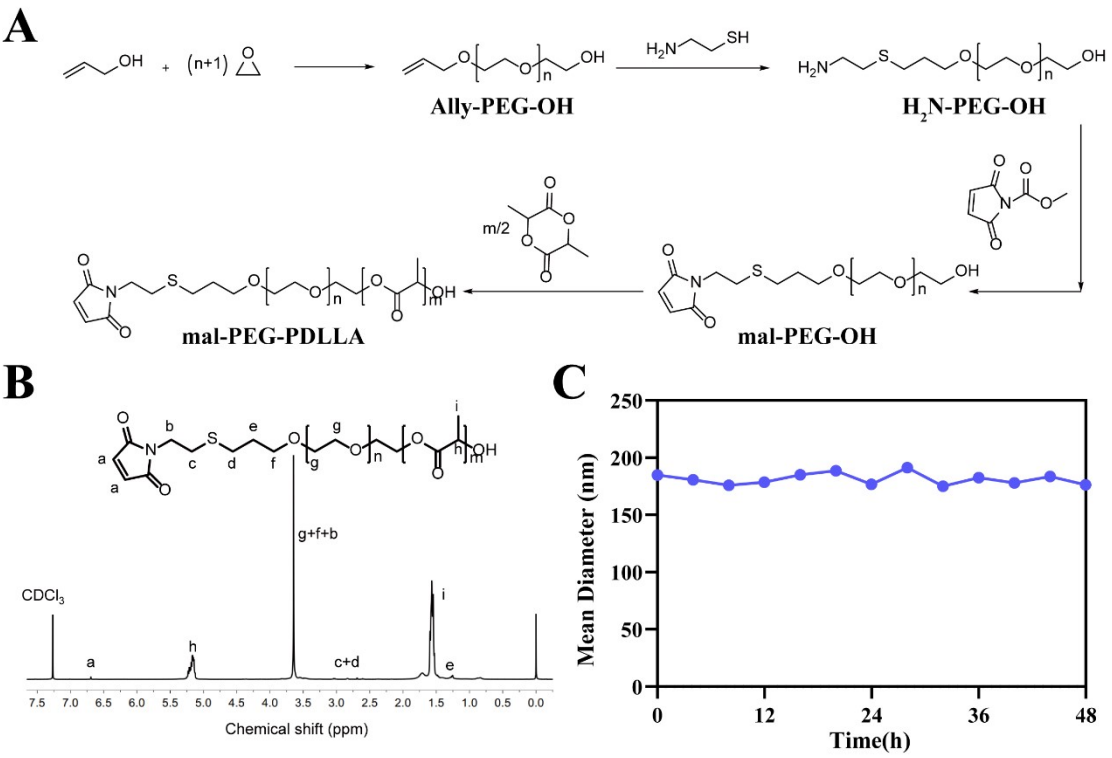

Figure S3. The synthesis and characterization of mal-PEG-PDLLA. A. the reaction pathway of of mal-PEG-PDLLA. B. ^{1}H NMR spectrum of mal-PEG-PDLLA in $CDCl_3$ at 25 ℃. Characteristic peaks of maleimide group, PEG and PDLLA were located at about 6.7 ppm, 3.6 ppm and 5.2 ppm (CH), 1.6 ppm (CH_3), respectively. C. The stability of scAb-ATO-NPs. The diameter of scAb-ATO-NPs varied between 160 and 190nm for 48 hours.

5.3 scAb-ATO-NPs inhibited PSCs activation more efficiently.

After treated with scAb-ATO-NPs, the expression of α-sma decreased more efficiently compared with both ATO and ATO-NPs groups, which means PSCs activation was inhibited. The similar decrease could be found in the expression of Collagen Type I and Fibronectin **(Fig. S4A)**. While co-cultured with the PSCs which were pre-treated with the scAb-ATO-NPs, the wound healing percentage of PANC-1/MIA PaCa-2 decreased most compared with other three groups **(Fig. S4B)**.

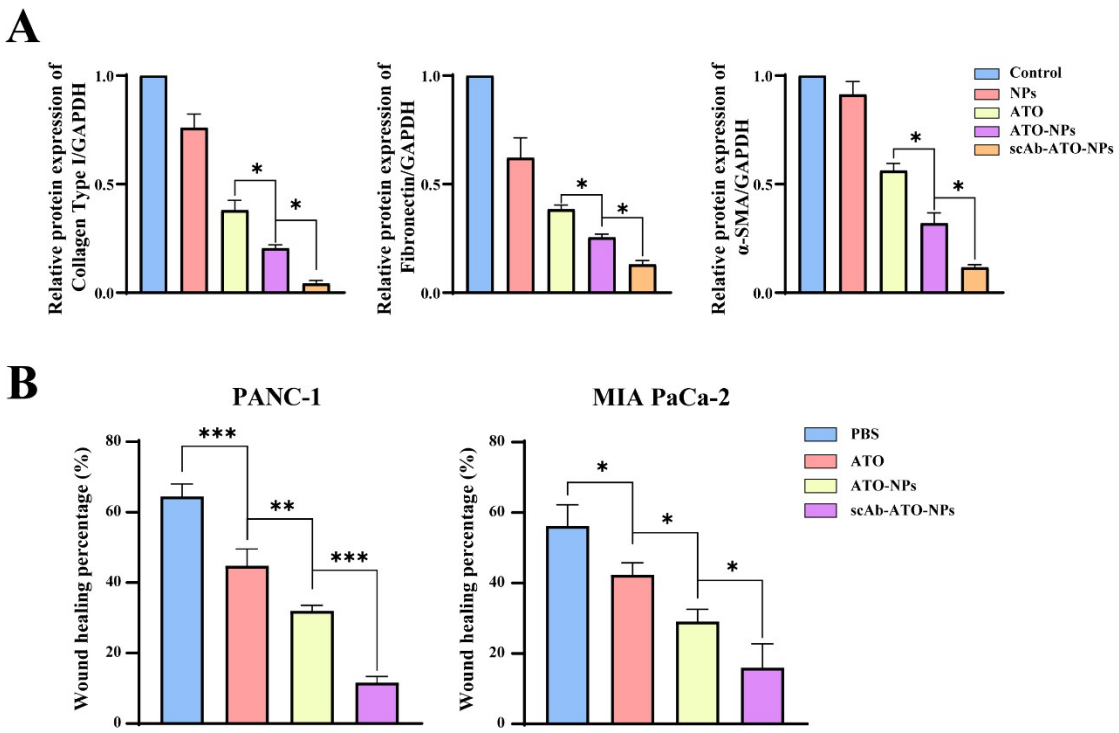

Figure S4. scAb-ATO-NPs inhibited PSCs activation. A. The protein expression in **Figure 6G** was quantified by Image J. B. The wound healing percentage was utilized to quantify the migration ability of PANC-1 and MIA PaCa-2. All the results were repeated for 3 times. *, $P < 0.05$; **, $P < 0.01$.***, $P < 0.001$.

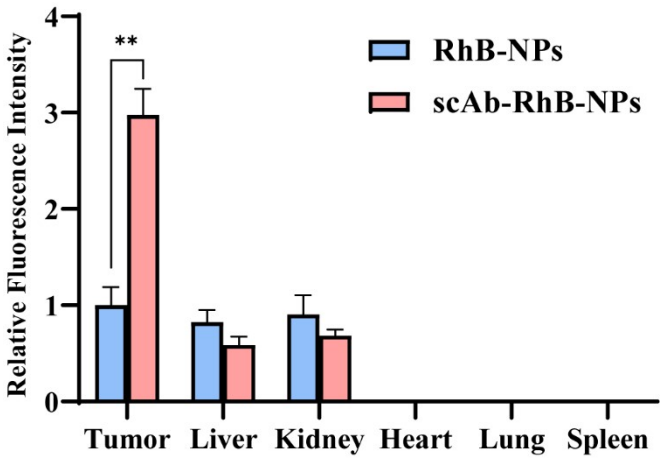

Figure S5. Quantitative analysis of the fluorescence in each organ by Image J software. tumors and organs were separated from tumor bearing mice received tail vein injection with RhB-NPs and scAb-RhB-NPs and aggregation and distribution of tumors and organs was recorded. The fluorescence intensity of tumors was significantly higher in mice administered scAb-RhB-NPs than in RhB-NPs (2.54-fold，$P < 0.01$).

5.4 the organ toxicity of the tumor-bearing mice received different treatments.

While treated with different drugs, no obvious organ injury could be found in the mice **(Fig. S6)**. The aspartate aminotransferase (AST), the alanine aminotransferase (ALT) and creatine level in the mice serum were detected to test the liver and kidney toxicity of scAb-ATO-NPs and no significant difference could be found **(Fig. S7).** These data demonstrated the biosafety of the synthesized nanoparticle, scAb-ATO-NPs**.**

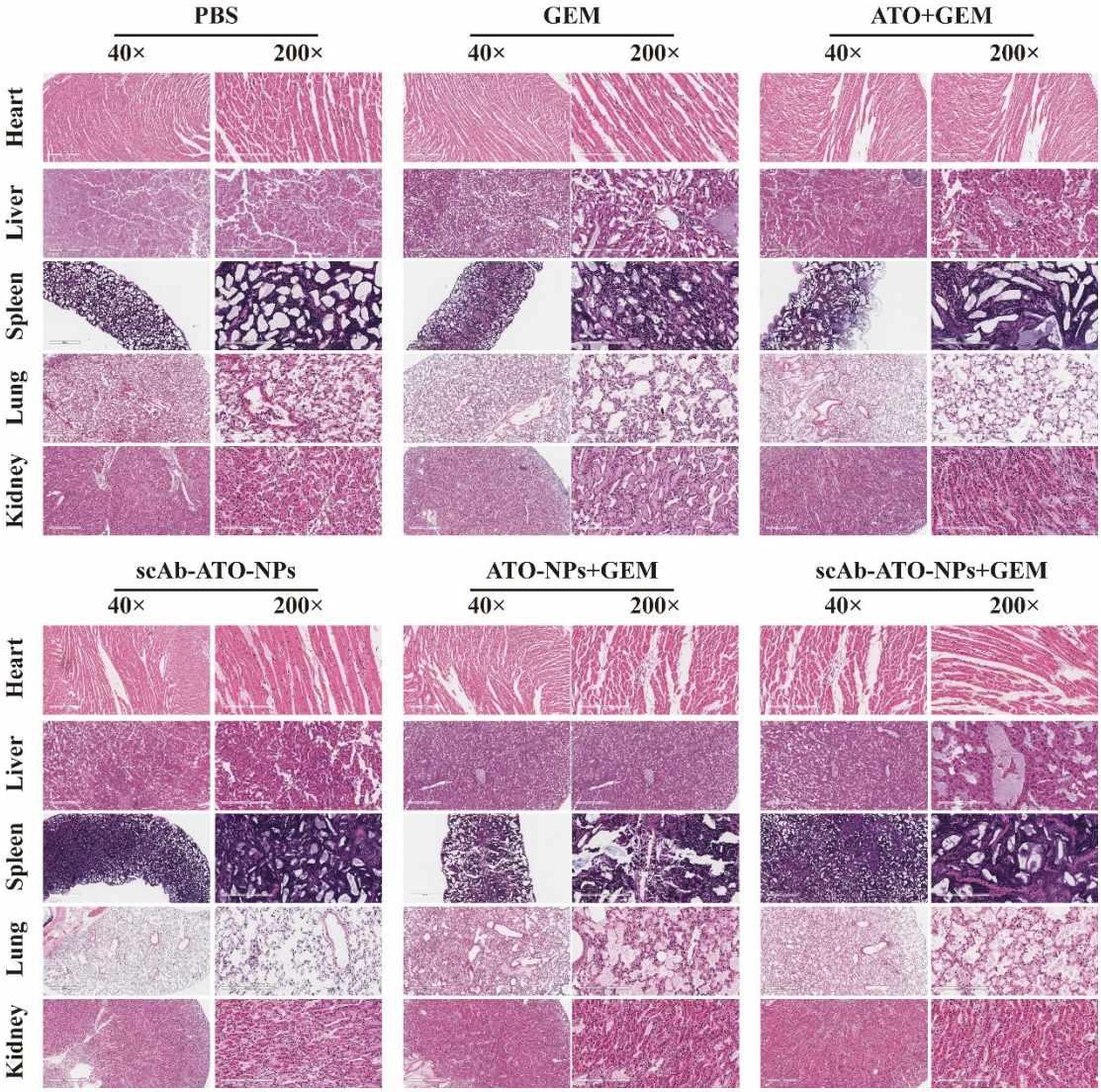

Figure S6 H&E staining of five organs. Morphological changes were not be observed after being treated with ATO of different formulations. Scale bars, 50μm.

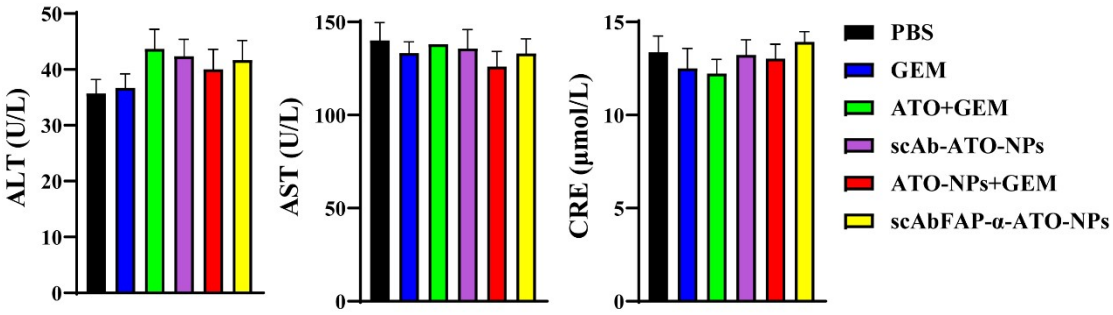

Figure S7 Serum test of BALB/c nude mice after treatments of scAb-ATO-NPs. AST, aspartate aminotransferase; ALT, alanine aminotransferase; CRE, creatinine. The data are presented as the MEAN (SD) (n = 3)